Garrido, S., Alvarez, D., Martin, F. & Moreno, L. (2019). An Anisotropic Fast Marching Method Applied to Path Planning for Mars Rovers. *IEEE Aerospace and Electronic Systems Magazine, 34(*7), 6–17.

DOI: 10.1109/maes.2019.2924124

An Anisotropic Fast Marching Method applied to Path Planning for Mars Rovers

Santiago Garrido, Fernando Martin, David Alvarez and Luis Moreno Robotics Lab. Carlos III University of Madrid, Spain
Email: {sgarrido,fmmonar,dasanche,moreno}@ing.uc3m.es

***Abstract*—This paper presents the application of the Anisotropic Fast Marching Method to the path planning problem of robots moving in spatial environments. The slope of a terrain should be considered in a tensorial way because at any point on a mountainside there are two main slopes: the maximum, which is the slope of the gradient, and the minimum, which is the slope iperpendicular to the gradient. The resulting trajectory of the path planning should take both into account so that the slopes in the trajectory are minimized, just as the Romans used flocks of cows to make Roman roads and so that the descent of the road was small as possible.**

I. Introduction

In recent times we are seeing an increase in space exploration by means of robots, such as Spirit or Opportunity on Mars, as well as the exploration of asteroids like Ceres or Vesta. For this reason it is necessary to have navigation and path planning systems that allow the robots to move safely and semi-autonomously, since the time necessary to transmit the information about the environment and send the orders of movement is very large.

In order to be able to move safely, the robot needs to have previous maps of the area, as well as those built from the data of its sensors and from them to calculate paths as safe as possible while taking into account the variation of altitude. It is important to note that most of the methods take the surface gradient at each point, rather than finding the gradient in the direction of the path (or its tangent).

This paper presents the application of the technique of the Anisotropic Fast Marching (AFM) to the calculation of trajectories that avoid obstacles while taking into account the variation of height and in the direction of the march. This technique has been used in computer graphics and computer vision to make anisotropic filters to perform sampling, segmentation, grouping or meshing. The novelty of the paper is its application to find outdoor paths in which the slope varies as slow as possible.

The Fast Marching method is based on the expansion of a wave, eg electromagnetic, in which the weight of the cost function represents the refractive index. The wave expands orthogonally to the wavefront, ie the expansion follows a vector perpendicular to the wavefront at each point of the wavefront. In previous articles we have discussed the path planning using the Fast Marching technique with a cost function that penalized the change of height, gradient and roughness. This time, we are going to study the application of the Anisotropic Fast Marching method to the resolution of this same problem using an anisotropic cost function.

To explain our goal, consider a mountainous landscape on Mars. At every point of the mountain, if the tangent plane is considered at that point, the AFM method calculates two vectors: the gradient or vector with the highest slope, and the least slope vector. These two vectors form a matrix or tensor field in which the slope in those two directions are the eigenvalues. In the AFM method, the expansion of the wave at each point of the wave front is done taking into account these two vectors of the tensor field giving more importance to one or the other depending on the anisotropy index.

The remainder of the paper is organized as follows. Section II shows the mathematical basis for the computation of shortest paths. Then, Section III introduces an explanation about the FMM and how this algorithm can be implemented. Next, Section VI presents numerical simulations that show promising results of the method. Finally, the main conclusions of this paper are summarized in section VII.

II. Riemannian Metric and Geodesic Distance

Geodesy is the science that studies how to measure distances, angles and shapes on a planet. In Differential Geometry, a geodesic is the path of minimum (generalised) distance between 2 points, measured on a generalised surface (Riemannian manifold), that is, the geodesics are the generalisation of the concept of line of minimum distance carried to Riemannian manifolds.

Intuitively, a differentiable manifold could be a space that is locally similar to $\mathbb{R}^n$. Riemannian manifolds are smooth manifolds equipped with Riemannian metrics (smoothly varying definitions of inner product on tangent spaces), which permit us to measure geometric quantities like distances and angles.

A (smooth) Riemannian manifold (M, g) is a real, smooth manifold M with an inner product g_p on the tangent space T_pM at each point p, and that varies smoothly from point to point. The family g_p of inner products is named a Riemannian metric (tensor).

The distance are often thought-about as a cost function that includes the slope in the different directions of the terrain.

Some examples are: Consider two points in $\mathbb{R}^2$, (x_1, x_2) and $(x_1 + dx_1, x_2 + dx_2)$ in cartesian coordinates. According to the theorem of Pythagoras

$$ds^2 = (dx_1)^2 + (dx_2)^2 \tag{1}$$

which is called the Euclidean metric. Now consider the surface of a sphere of radius r, being its equation

$$\begin{aligned}\mathbf{X}(\theta,\phi) &= r\sin(\theta)\cos(\phi) \\ &+ r\sin(\theta)\sin(\phi) \\ &+ r\cos(\theta)\end{aligned} \tag{2}$$

where θ and ϕ are the polar angles. The displacement between two points located on the surface of the sphere: $\mathbf{X}(\theta,\phi)$ and $\mathbf{X}(\theta+d\theta,\phi+d\phi)$ is

$$d\mathbf{X} = \partial_\theta \mathbf{X} d\theta + \partial_\phi \mathbf{X} d\phi \tag{3}$$

In this case, the square of the length of the infinitesimal segment connecting this two points is given by

$$\begin{aligned}ds^2 &= (d\mathbf{X}d\mathbf{X}) \\ &= |\partial_\theta \mathbf{X}|^2 (d\theta)^2 + 2\partial_\theta \mathbf{X}\partial_\phi \mathbf{X} d_\theta d_\phi + |\partial_\theta \mathbf{X}|^2 (d\phi)^2 \\ &= g_{11}(d\theta)^2 + g_{12}d\theta d\phi + g_{21}d\phi d\theta + g_{22}(d\phi)^2 \\ &= g_{ij}d\theta d\phi\end{aligned} \tag{4}$$

In the case of our application, we have a Mars surface that can be considered as differentiable manifold embedded in R^3, composed by a set of compatible maps, each one of them is an application from $[0,a]x[0,b]$ to a patch M^2 in $\mathbb{R}$.

We can consider one of this maps, and a curve $u = u(t),\ v = v(t)$ defined in the parametric domain $[0,a]\times[0,b]$, then $\mathbf{r} = \mathbf{r}(u(t),v(t))$ is a curve lying in the surface. The tangent vector to the curve can be calculated by differentiating with respect to t:

$$\dot{\mathbf{r}}(t) = \mathbf{r_u}\dot{u} + \mathbf{r_v}\dot{v} \tag{5}$$

where $\mathbf{r_u}, \mathbf{r_v}$ are the partial derivatives with respect u and v.

The tangent plane at point P consist on all the tangent vectors, with an expression as equation 5 for any smooth curve passing trough P. As any tangent vector to the surface at point P is a linear combination of $\mathbf{r_u},\ \mathbf{r_v}$, the equation of T_p can be written as

$$\mathbf{T}_p(\mu,\nu) = \mathbf{r}(u_p,v_p) + \mu\mathbf{r}_u(u_p,v_p) + \nu\mathbf{r}_v(u_p,v_p) \tag{6}$$

where μ, and ν are parameters.

The linear part of the growth of the arc length is defined by the first fundamental form of the surface

$$I = ds^2 = d\mathbf{r}^2 = E(u,v)du^2 + 2F(u,v)dudv + G(u,v)dv^2 \tag{7}$$

The notation

$$g_{11} = E,\ g_{12} = F,\ g_{22} = G$$

is often used. With this notation, the square of the length of the curve $r(t)$ is

$$L^2(r(t)) = \int_{t_1}^{t_2} g_{ij}du_i du_j = \int_{t_1}^{t_2} [dudv] \begin{bmatrix} g_{11} & g_{12} \\ g_{12} & g_{22} \end{bmatrix} \begin{bmatrix} du \\ dv \end{bmatrix}$$

Intuitively, the first fundamental form tells how to calculate the distances along the paths within the surface.

The crucial point in this development was the contribution of Gauss who affirms that the intrinsic geometry of a surface S depends entirely and completely on the first fundamental form. In other terms, we will conclude that the geometrical properties of a surface S are often considered independent of the geometry of the Euclidean space that contains the surface, since that only needs the definition of an inner product for tangent vectors to the surface (first fundamental form).

Now, we can calculate in each point of the surface, the gradient and its normal vector instead of using $\mathbf{r}(u)$, and $\mathbf{r}(v)$.

This gave us a tensor field $T(x)$ of dimensions (n,n,2,2), that it is the structure tensor field of the image map. The sign ambiguity can be removed by tensorizing the gradient [11], [12].

The tensor $T(x)$ can be diagonalized to obtain the directions of maximum growth (that of the gradient) and the orthogonal direction given by the minimum growth (in absolute value). This can be done using the eigendecomposition of the corresponding matrix

$$T(x) = Q(x)H(x)Q^{-1}(x)$$

where $Q(x)$ is the orthogonal square $(N\times N)$ matrix whose i^{th} column is the eigenvector $e_i(x)$ of $T(x)$ and $H(x)$ is the diagonal matrix whose diagonal elements are the corresponding eigenvalues $\lambda_i(x)$.

$$\begin{aligned}&H(x) = \lambda_1(x)e_1(x)e_1(x)^T + \lambda_2(x)e_2(x)e_2(x)^T \\ &\text{with} \quad 0 \le \lambda_1, \lambda_2\end{aligned} \tag{8}$$

using matrix notation the expression is

$$\begin{aligned}H(:,:,1,1) &= \lambda_1.*e_1(:,:,1).^2 + \lambda_2.*e_2(:,:,1).^2; \\ H(:,:,1,2) &= \lambda_1.*e_1(:,:,1).*e_1(:,:,2) \\ &\quad + \lambda_2.*e_2(:,:,1).*e_2(:,:,2); \\ H(:,:,2,1) &= H(:,:,1,2); \\ H(:,:,2,2) &= \lambda_1.*e_1(:,:,2).^2 + \lambda_2.*e_2(:,:,2).^2;\end{aligned} \tag{9}$$

being $e_1(x)$ y $e_2(x)$ the eigenvectors (un-oriented) in the directions of minimum and maximum growth (in absolute value) and $\lambda_1(x)$ and $\lambda_2(x)$ are the eigenvalues and represent the measure of such growth in those two directions .

If instead of using the eigenvalues $\lambda_1(x)$ and $\lambda_2(x)$, we use 1, $1/\alpha(x)$, we are giving more or less importance to an eigenvector or the other. In this case, the metric changes with $\alpha(x)$, or in other words, it has been defined a cost function, and the method solves the variational problem of finding the path with fixed origin and final points that minimizes this cost function.

In other words, the new tensor is

$$\begin{aligned}&H(x) = 1e_1(x)e_1(x)^T + \frac{1}{\alpha(x)}e_2(x)e_2(x)^T \\ &\text{with} \quad 0 \le \lambda_1, \lambda_2\end{aligned} \tag{10}$$

The anisotropy of the metric $H(x)$ is defined as

$$\begin{aligned}&\alpha(x) = \frac{\lambda_1-\lambda_2}{\lambda_1+\lambda_2} = 2\frac{\sqrt{ab-c^2}}{a+b} \in [0,1], \\ &\text{for} \quad H(x) = \begin{pmatrix} a & c \\ c & b \end{pmatrix}\end{aligned} \tag{11}$$

This means that the shortest paths in this metric are those which tend to have the direction of the vector normal to the gradient and tangent to the level lines.

III. The Eikonal Equation and the Fast Marching Planning Method

In robotics, the path planner of the mobile robot must drive it in a smooth, safe and fast way to the goal point. In nature, there are phenomena that work in the same way, such as electromagnetic waves. If at the goal point there is an antenna that emits an electromagnetic wave, then the robot could drive itself to the destination following the waves to the source. The idea of the electromagnetic wave is especially interesting because the potential magnetic field has all the good properties desired for the trajectory, such as smoothness (that is, C^{∞}) and the absence of local minima.

In a similar manner, Fermat's principle in optics says that the path of a beam of monochromatic light follows the path of least time. When the index of refraction is constant, the wavefronts are circles, which represent the different arrival times, and the rays are straight lines. In the case of two media with different indices of refraction, rays are bent as shown in the left side of figure 1, resulting in the refraction of the path, known as Snell's law effect. In the case that the refractive index varies continuously, the light beam is also continuously bend, as shown in in the right side figure 1.

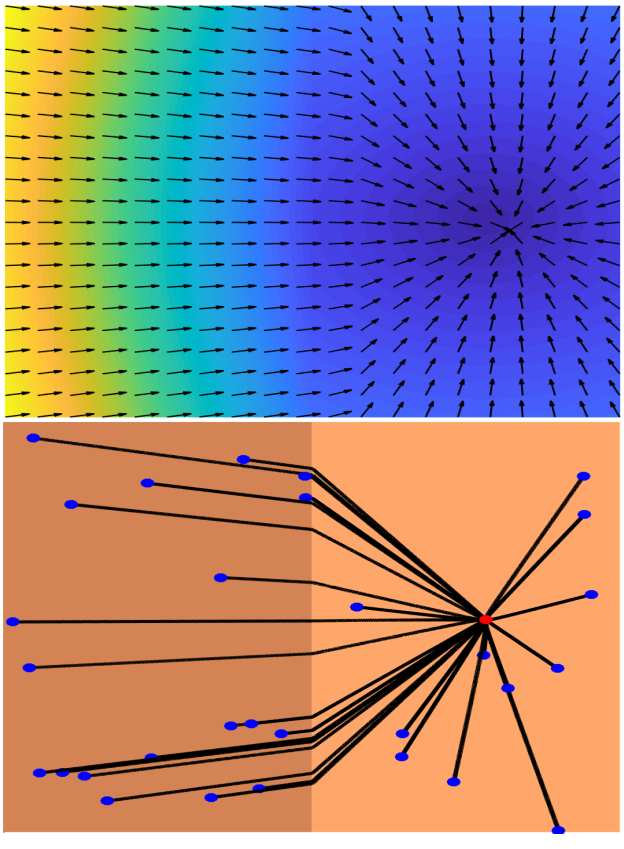

Fig. 1. a) Potential and its vectorial field obtained with the Fast Marching Method when there are two media of different refractive indexes (air and water, for example) and b) its corresponding light rays or paths.

One way to characterise the position of a wavefront in expansion is to compute the arrival time T, in which the front reaches each point of the space. It is evident that, for one dimension, we can obtain the equation of the arrival function T in an easy way, simply considering the fact that the distance x is the product of the speed F and the time T.

$$x = F \cdot T \tag{12}$$

Then, the spatial derivative of this function becomes the gradient as:

$$1 = F\frac{dT}{dx} \tag{13}$$

and therefore, the magnitude of the gradient of the arrival function $T(x)$ is inversely proportional to the speed:

$$\frac{1}{F} = |\nabla T| \tag{14}$$

For multiple dimensions the same concept is valid, since the gradient is orthogonal to the level sets of the arrival function $T(x)$. In this way, we can characterize the movement of the front as the solution of a boundary conditions problem. If speed F depends only on the position, then equation 14 can be reformulated as the Eikonal equation:

$$|\nabla T|\, F = 1. \tag{15}$$

The Fast Marching method is a numerical algorithm for solving the Eikonal equation, originally on a rectangular orthogonal mesh, introduced by Sethian in 1996 [1]. The FMM is an $O(n)$ algorithm, as demonstrated in [2], where n is the total number of grid points. The algorithm relies on an upwind finite difference approximation to the gradient as a first order solution of the differential equation.

The FMM is used for problems in which the speed function never changes of sign, and so the wave front is always moving forwards (there are no reflections). This allows us to transform the problem into a stationary formulation, because the wave front crosses each grid point only once. The wave propagation given by the FMM gives us a distance function that corresponds to the Geodesic distance measured with the metric given by the the refraction matrix, which indicates the velocity at which the wave front moves forward.

Since its introduction, the FMM has been applied with success to a wide variety of problems that arise in geometry, computer vision and manufacturing processes (see [3] for details). Several advances have been made to the original technique, including the adaptive narrowband methodology and the FM method for solving the static Eikonal equation [1], and also different implementations have been tried out to make it faster [4].

A. Algorithm Implementation on an Orthogonal Mesh

The Fast Marching Method models any phenomena that can be described as a wave front propagating normal to itself with a speed function $F = F(i, j)$. The main idea is to methodically build the solution using only upwind values. Let $T(i, j)$ be

the time at which the curve crosses the point (i, j), then it satisfies $|\nabla T|F = 1$, the Eikonal equation.

In order to understand how fast marching works, imagine an imprudent visitor that leaves unextinguished fire at some location in a natural reserve. The flame quickly becomes a forest fire, which expands outwards. Fire consumes the reached trees so the fire always propagates forward. We can record the fire front position at different points in time. It appears that the fire traverses the route having the smallest propagation time (and hence, the shortest length if the velocity is constant). In optics and acoustics this fact is known as Fermat's principle or, in a more general form, the least action principle. In plain language, Fermat's principle states that light traveling between two points always chooses the quickest path. Snell's law of refraction follows directly from this principle.

It is important to point out that the propagation happens from smaller to bigger values of T. While evolving, the algorithm classifies the points of the mesh into three sets: frozen, open and unvisited. Frozen points are those where the arrival time has been computed and is not going to change in the future. Unvisited points are those that have not been processed yet. Finally, open are those points belonging to the propagating wave front, which can be considered as an interface between frozen and unvisited regions of the mesh. Initially, the source X_s is marked as frozen and assigned a time of arrival or 0. All points adjacent to it (von Neumann neighbourhood is considered), are marked as open and their value is computed using equation 16.

$$\left(\frac{T - T_{\mathrm{x}}}{\Delta x}\right)^2 + \left(\frac{T - T_{\mathrm{y}}}{\Delta y}\right)^2 = \frac{1}{F_{\mathrm{ij}}^2} \tag{16}$$

At each iteration, the open point with the smallest value of $T(x)$ is labeled as frozen and its neighbours are analysed and tagged as open. The process continues until all points are marked as frozen or the goal is reached.

Figure 2 a) explains evolution of the method: in the first subfigure the dark blue point is the start point of the wave, and its neighbours are marked in grey. In the 2nd subfigure, their value T is computed and they are coloured in light blue, while their neighbourhoods are labeled in grey. The algorithm continues and the points with different time of arrival are marked with a different colour. If one plots the final solution, using the time of arrival as the third axis, the funnel potential with one global minimum shown in figure 2 b) is obtained.

IV. Anisotropic Fast Marching

The Anisotropic Fast Marching method uses an structure tensor field that acts as the anisotropic metric in the computation. In that field, the main eigenvector is aligned with the gradient and the second eigenvector is aligned with the normal to the gradient. In the case of a mountainous environment, as in the case of Mars, these vectors represent the directions of maximum slope (gradient) and minimum slope (normal). Then, the tensor field is managed by the coefficient of anisotropy, which gives the importance given to the main eigenvector field with respect to the second eigenvector field according to

$$\alpha(x) = \frac{\lambda_1 - \lambda_2}{\lambda_1 + \lambda_2} \tag{17}$$

The new metric is given by the tensor field corresponding to the given eigen-decomposition

$$H = l_1 * e_1 * e_1' + l_2 * e_2 * e_2' \tag{18}$$

where e_1 is the main eigenvector, e_2 is the second eigenvector, l_1 is the first eigenvalue and l_2 is the second eigenvalue.

This metric can be usefully applied to the path planning problem. Given a height map of and complex environment, like in Mars, the tensor field based on height changes can be easily computed. Then, the goal point of the robot is set as the starting point of the wave expansion, note that this forces this point to be the only global minimum of the resulting map. The propagation of the wave is done taking into account: the angle of the front propagation with respect to the tensor filed at that point and the anisotropy index selected by the user. This index indicates how much the robot should avoid changing the height along the path. When the computation has finished, the result is the D matrix or second potential which indicates the time of arrival of the wave at each point. Since the goal point is the global minimum, the gradient method is applied starting as the actual location of the robot, which lead to the shortest possible path (according to the given metric).

V. Estrategias multirobot

El uso de tecnicas basadas en Fast Marching tienen la ventaja de que se puede modificar la metrica subyacente para usarla para resolver problemas multirobot.

Para ello consideremos una zona mas o menos plana. Si al mapa de alturas f le sumamos una pequeña gaussiana en la posición de otro robot, al calcular el campo tensorial tendremos una zona con valores grandes que al calcular la expansion de la onda, el metodo tratara de evitar. Es decir, el camino del primer robot intentara evitar la posicion del segundo robot.

Por otro lado, tambien se pueden abordar problemas de formaciones, como pueden ser conjuntos de robots en una cierta configuracion para explorar una cierta region. Para ello, se puede usar el hecho de que los metodos basados en Fast Marching funcionan como un doble campo sin minimos locales: atractivo hacia el objetivo y repulsivo hacia o desde los obstaculos. Si el robot lider tiene asociada una formacion geometrica flexible dada por un conjunto de nodos, y si cada robot tiene como objetivo local cada uno de esos nodos, conseguimos un movimiento conjunto suficientemente flexible y que se ajuste a la formacion con una repulsion de los posibles obstaculos.

VI. Numerical Simulations

The algorithm is tested using a height map obtained from satellite measurements of Mars. In this environment, several tests have been carried out in order to test the usability of the algorithm and exploring the different behaviours that can be achieved when the parameters are changed.

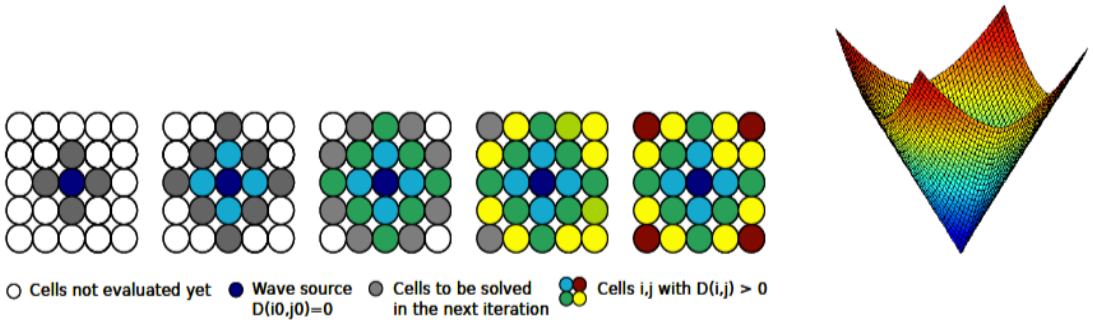

(a) Iterations of FM with one wave in 2D.

(b) Time of arrival potential $D(\mathbf{x})$ (third axis)

Fig. 2. Scheme of Fast Marching propagation with an initial point. Different colours (blue to red) represent different arrival times in increasing order.

Figure 3 shows the adaptation of a path to the terrain following the tensorial field. It can be seen how the path has the least possible changes in height from the starting to the goal point. The first image shows the height map and the computed path. The second one includes the tensor field computed from the height map and based on its gradient, which is shown in the third image. In the fourth one the Normal components of the gradient are indicated. Finally, a 3D view of the environment and the computed path are included.

The adaptation to the terrain can be more or less strict depending on the anisotropy index set by the user. The next simulation shows how this index can influence the path computed by the algorithm. Figure 5 shows this influence using the next values for the Anisotropy index: 0.01, 0.03 and 0.05. The first image shows the path with less changes in height, however, the path includes abrupt turns. When the index is augmented, the path has more altitude changes but gets smoother, being the third best one the best option in this case, with index $a = 0.05$. Figure **??** shows the Different paths in the Mars dunes using the AFM method for an anisotropy coefficient of 0.03 and

Figure 6 shows different paths in the uplift of layered materials from the intersection of two craters of Mars using the AFM method for an anisotropy coefficient of 0.03. Then, figure 10 includes: a) the height map of the environment with the computed Anisotropic Fast Marching path following the the peaks of the area; the mean curvature of the environment; and two quality measurements of the path shown in a), c) the height changes and d) the curvature changes along the path.

Figure 12 shows The adaptation of the AFM paths to the level lines is better when importance of the normal eigenvector field is higher (smaller anisotropy index). Left: Height of terrain that consists in mountain (upper view) and a typical path between two points and right: AFM expansion, normal vectorial field and path, for anisotropy indexes of 0.3, 0.06 and 0.03.

First, the use of the anisotropic index is explained using figure VI. Left column shows a height map in which higher altitudes are represented by a dark blue colour, lighter blue areas represent lower altitudes and green and yellow ones are the lowest. The map reproduces an artificial mountain in which the different height levels form perfect circles (with equation $z = -(x^2 + y^2)$). Besides, the computed path is represented by a red line. It is important to note that the initial and the goal points are at the same height. Finally, the vectors on top of the height map follow the lines indicating the same height, which corresponds to a field which is perpendicular to the gradient. The right column shows the arrival times for the evolution of the wavefront. The colours change gradually when the time increases. This figure allows to appreciate the power of adaptation of the method in order to find paths which tend to minimize the height change. This adaptation to the terrain can be more or less strict depending on the anisotropy index.

It is important to appreciate the different shapes formed due to the way the wavefront advances. These differences are provoked by the different values of the anisotropic index (0.3, 0.06 and 0.03 respectively). It can be appreciated that when the anisotropic index is higher, the computed path traverses the environment more directly, follow the gradient field. On the contrary, when it is smaller, the path follow the height levels, minimizing the height changes.

Then, the behaviour of the computed paths is analyzed quantitatively. Two main characteristics are taken into account: the height changes and the curvature of the terrain traversed. The former is directly extracted from the height map.

In 7a, the heights of the trajectories of figure 4 for the anisotropic indexes 0.01, 0.03 and 0.05 are shown. Using these heights of the three paths, its possible to calculate the undershoot of the heights of the three paths for the different anisotropy values as shown in table II. In 7a can be appreciated that the maximum gradients are similar for the three curves.

TABLE I
UNDERSHOOT OF THE HEIGHT OF THE PATHS

Anisotropy	Minimum	Percentage undershoot
0.03	0.025	15.0
0.06	0.055	31.4
0.3	0.125	71.4

For the curvature, it can be studied using the curvature of the surface in the points of the path: i,e, the Gaussian and mean curvature, and the curvature of the path as a 3D curve.

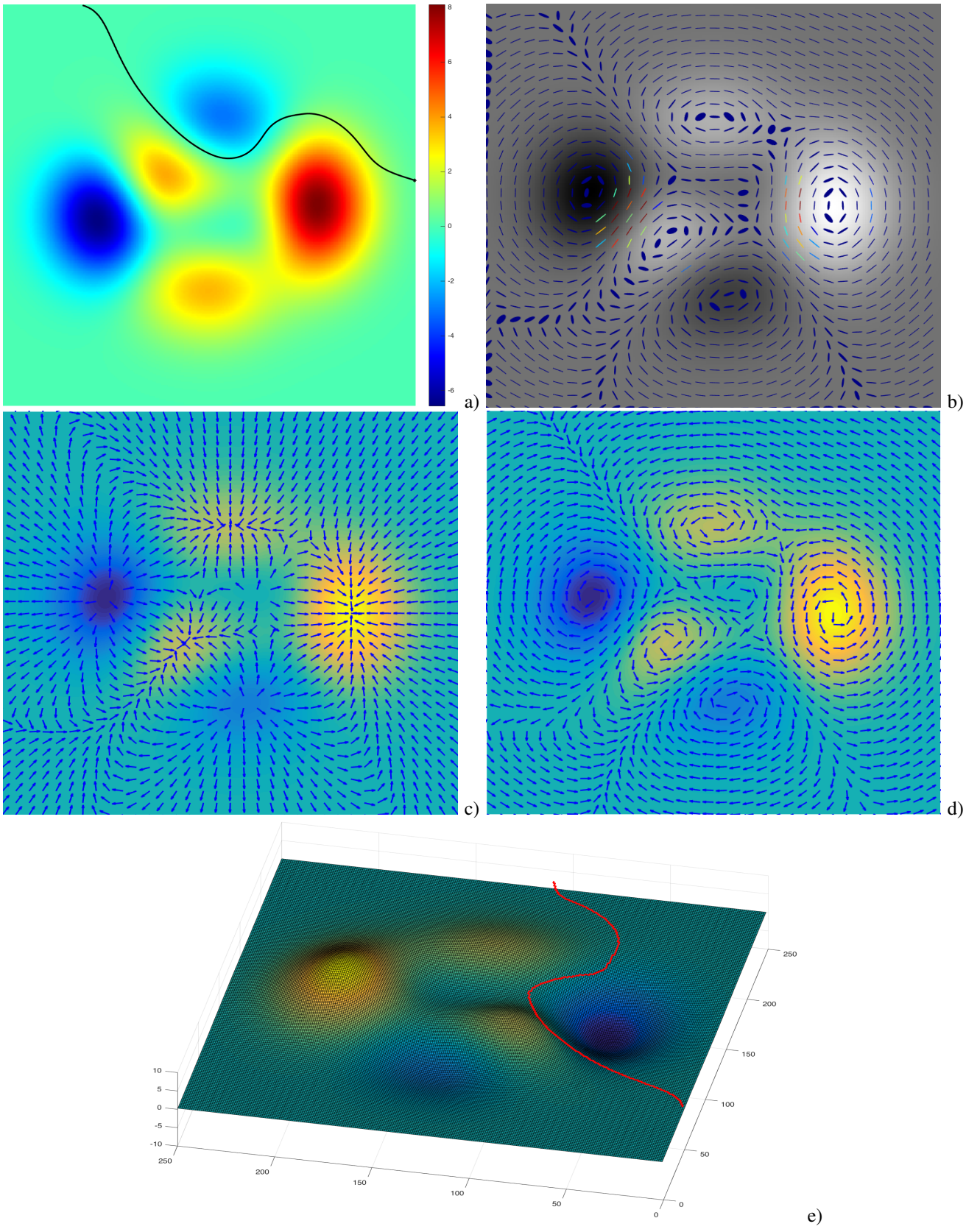

Fig. 3. a) Typical Anisotropic Fast Marching path with small changes in height, b) Tensorial field associated to this map, c) and d) Gradient and Normal components of the tensorial field, and e) 3D plot of the same map and computed path.

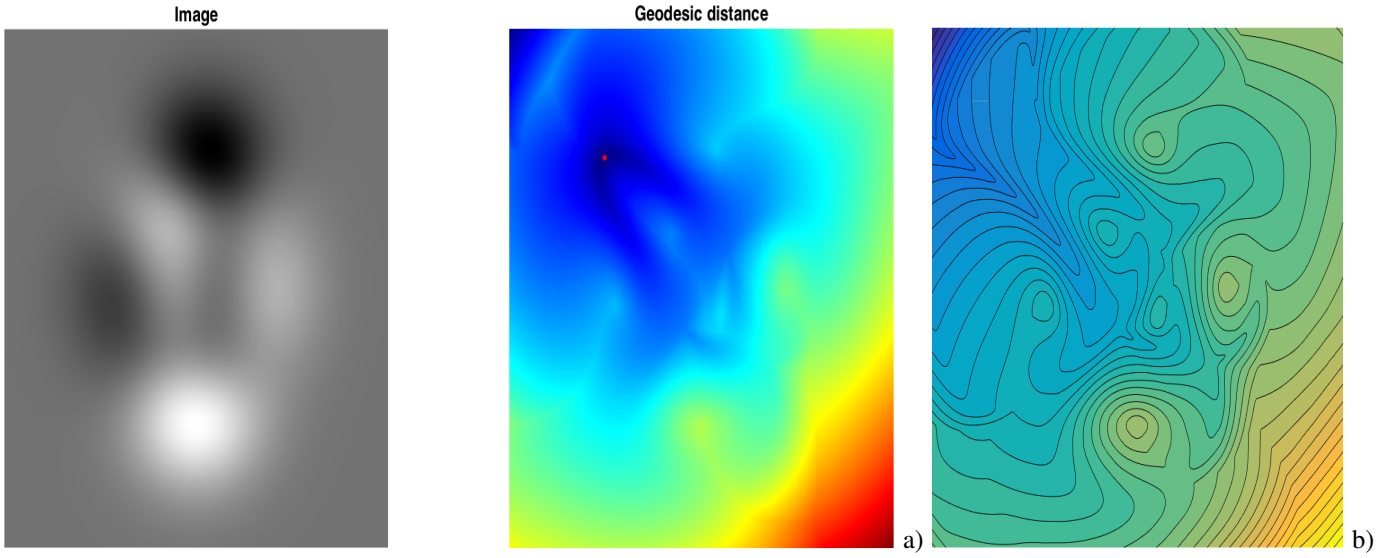

Fig. 4. Grey level height map (1st potential) used as input and two representations of the propagation of the Anisotropic FM wave expansion (2nd potential)

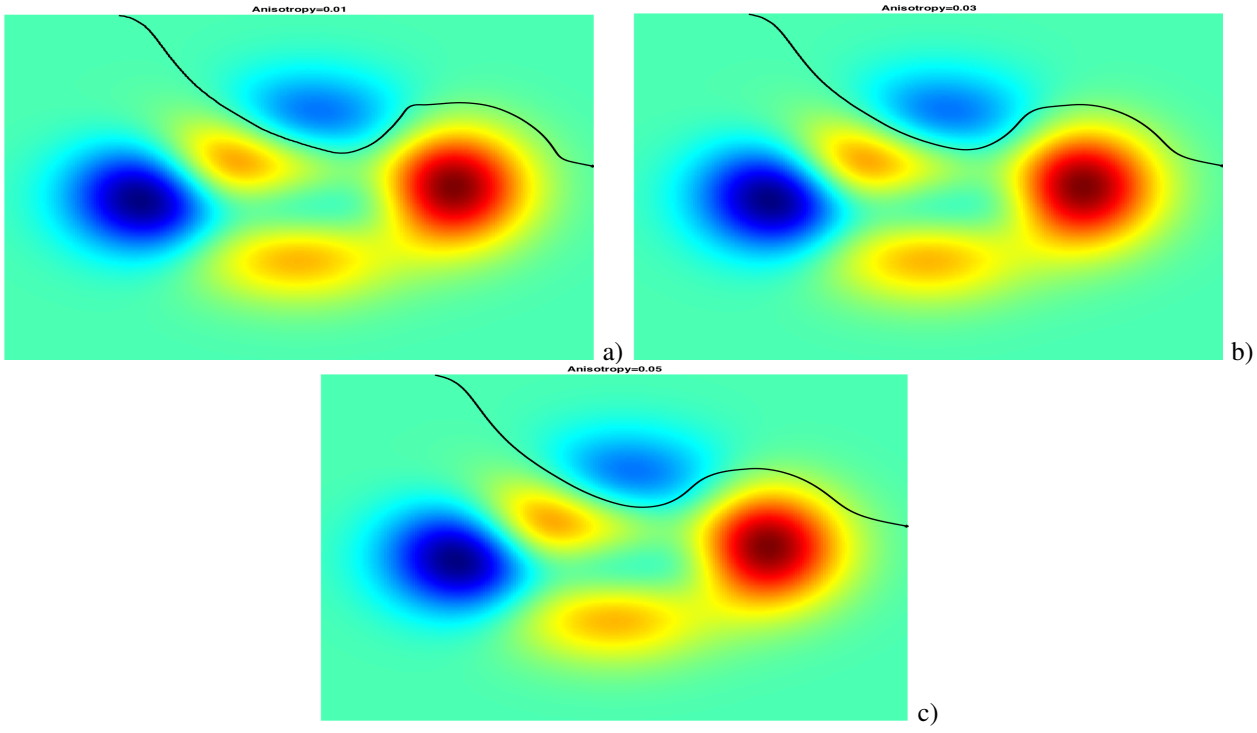

Fig. 5. Influence of the Anisotropy coefficient λ in the path for three values: 0.01, 0.03 and 0.05. The first has less changes in height, the last is smoother a λ= 0:03 is the best option: it has small changes in height and is quite smooth.

In order to study the surface curvature is necessary to define the normal vector and the second fundamental form.

The normal vector to the surface in the point P, given by $\mathbf{r} = \mathbf{r}(u(t), v(t))$ is

$$\mathbf{n} = \frac{\epsilon[\mathbf{r}_u, \mathbf{r}_v]}{|[\mathbf{r}_u, \mathbf{r}_v]|} \tag{19}$$

where ϵ is 1 if $\{\mathbf{r}_u, \mathbf{r}_v, \mathbf{n}\}$ has right-hand orientation and -1 if it has left-hand orientation.

The second fundamental form is

$$II = [\mathbf{r}_{uu}, \mathbf{n}]du^2 + 2[\mathbf{r}_{uv}, \mathbf{n}]dudv + [\mathbf{r}_{vv}, \mathbf{n}]dv^2 \tag{20}$$

$$= Ldu^2 + 2Mdudv + Ndv^2 \tag{21}$$

The second fundamental form describes how ”curved” is the embedding surface.

At any point on a surface, the normal vector is computed, and planes containing this normal vector are called normal planes. The curve formed at the intersection of every plane with the surface is computed, from which the curvature is extracted. Among them, the maximum and minimum values

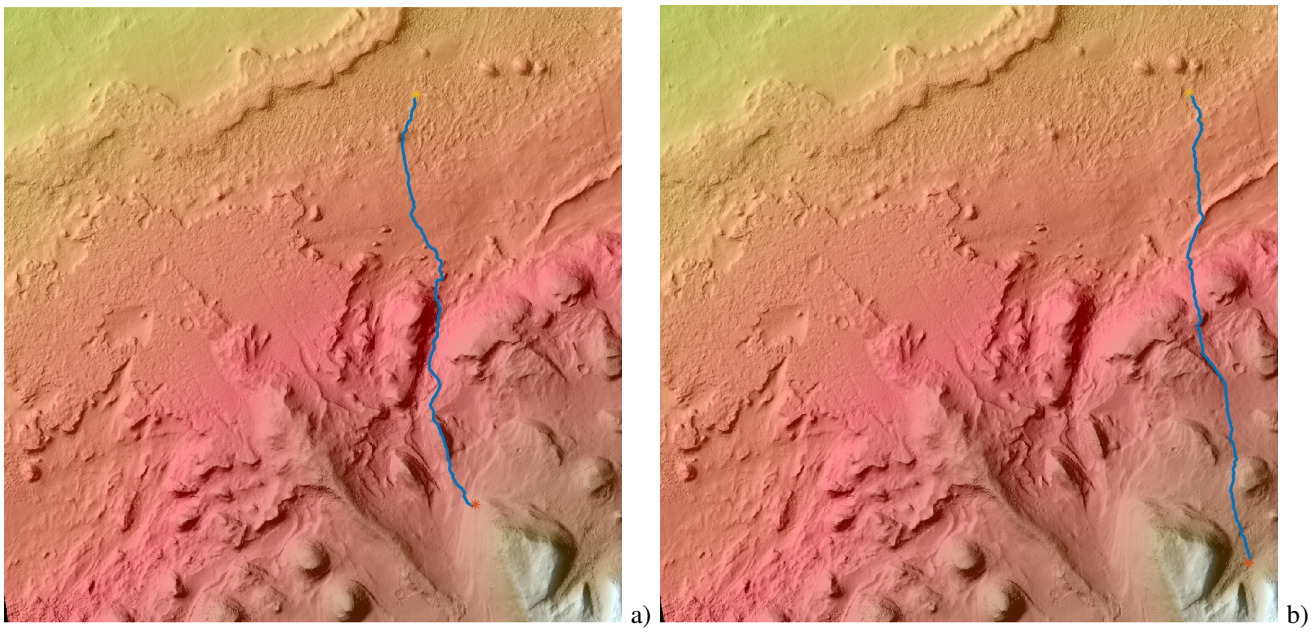

Fig. 6. Different paths in the Uplift of Layered Materials From the Intersection of Two Craters of Mars using the AFM method for an anisotropy coefficient. of 0.03.

of these are called the *principal curvatures*, commonly names as k_1 and k_2. Then, the Gaussian curvature is the product of the two principal curvatures:

$$K = k_1 * k_2. \tag{22}$$

The mean curvature at each point is defined as the average signed curvature over intersecting planes, however, by applying Euler's theorem, this is equal to the average of the principal curvatures:

$$H = 0.5 * (k_1 + k_2) \tag{23}$$

The explicit formulae for H and K are:

$$K = \frac{LM - N^2}{EG - F^2}, \qquad H = \frac{LG - 2MF + NE}{2(EG - F^2)} \tag{24}$$

The Bonnet theorem ensures that (under certain conditions) these two fundamental form uniquely characterize the surface.

In order to study the curvature of paths as 3D curves, they can be considered as regular curves in three dimensions. If $\gamma(s)$is parametized by the arc length, then the unit tangent vector $\mathbf{T}(s)$ as $\mathbf{T}(s) = \gamma'(s)$ and the curvature is the magnitude of the acceleration

$$\kappa(s) = ||\gamma''(s)|| \tag{25}$$

The curvature measures the twisting of the Frenet frame.

In Cartesian coordinates, the curvature of the curve $\gamma(t) = (x(t), y(t), z(t))$, not necessarily parametrized by its arc length is

$$\kappa = \frac{\sqrt{(z''y' - y''z')^2 + (x''z' - z''x')^2 + (y''x' - x''y')^2}}{(x'^2 + y'^2 + z'^2)^{\frac{3}{2}}} \tag{26}$$

where the prime means differentiation with respect to t.

TABLE II
UNDERSHOOT OF THE HEIGHT OF THE PATHS

Anisotropy	Gaussian Curvature	Mean Curvature	Max-Max Curvature	Max-Min Curvature
0.03	0.03	0.3	0.6	0.05
0.06	0.05	0.35	0.7	0.07
0.3	0.25	0.63	1.0	0.26

Figure 7 shows a comparison of the behaviour of the different paths shown in figure VI, for different values of the anisotropy index: 0.3, 0.06 and 0.03. At the top, the hight changes can be appreciated. As commented before, as the anisotropic index is larger, the path tends to follow the gradient vector field, which provokes the path to traverse more height changes from the initial to the goal point (yellow line). As the index becomes smaller, the path tends to follow the height level lines, and only traverse different hight areas when it is really necessary (blue line). This behaviour greatly affects the terrain the robot traverses when following the path, as indicated by the bottom images of figure 7, which represent the Gaussian and mean curvatures, respectively. As expected, when the gradient of the height map is followed, the curvature of the terrain traversed is greater, which indicates the robot will have more difficulties to follow it.

Figure 8 shows the application of this method to a more realistic terrain. At the top, a 3-dimensional view of the environment is shown, in which mountains are represented in blue and purple, while valleys are depicted in green and yellow. In this case, the starting and goal points are at the same height, but the terrain in between is very sharply sloped. The computed path is also plotted as a black line. The second image in the figure is a 2D projection of the map which includes the height level lines and the path. It is important

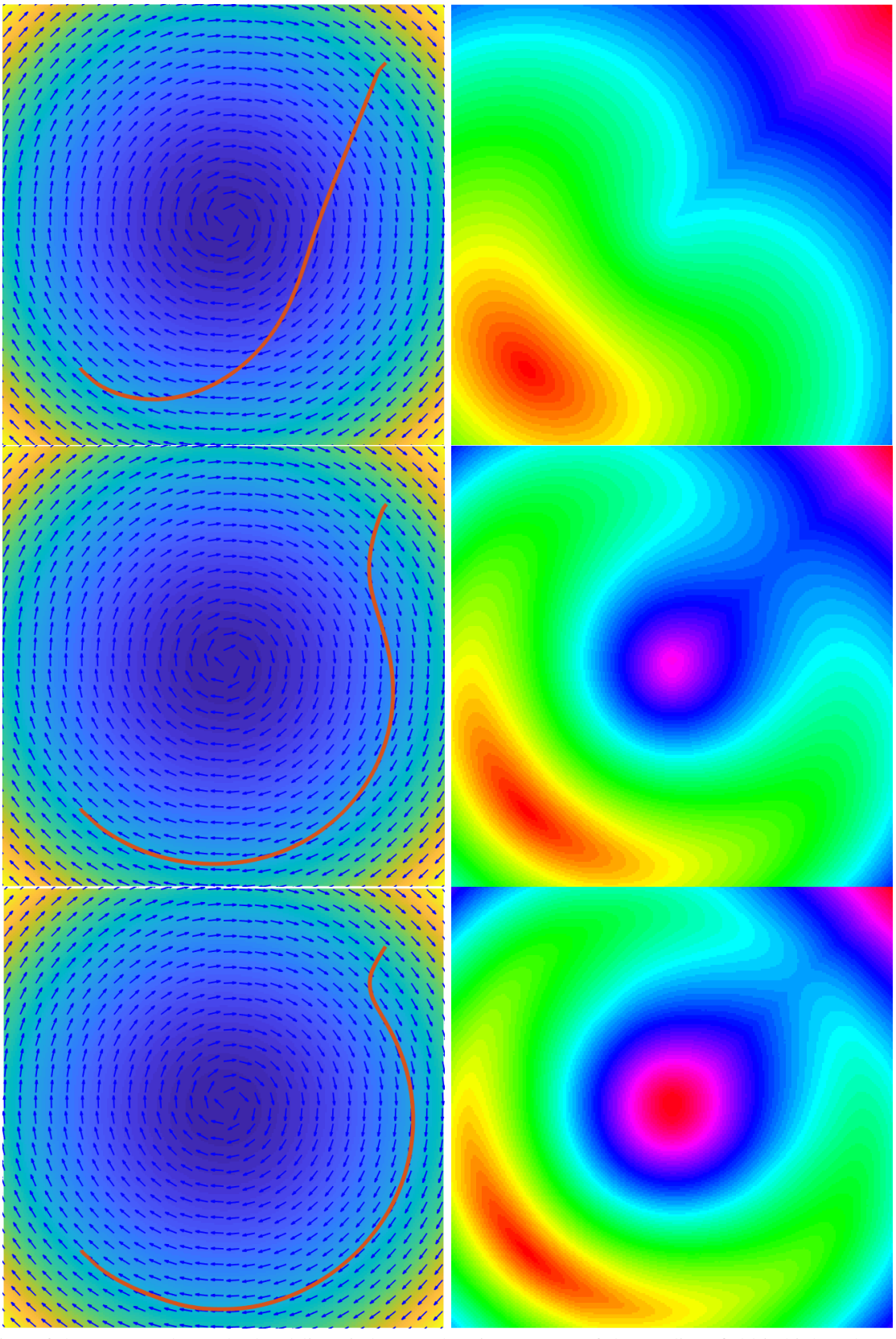

The adaptation of the AFM paths to the level lines is better when importance of the gradient field is higher (larger anisotropy index). Left: Height of the terrain and path and, right: AFM expansion, normal vectorial field and path, for anisotropy indexes of 0.3 (top), 0.06 (center) and 0.03(bottom).

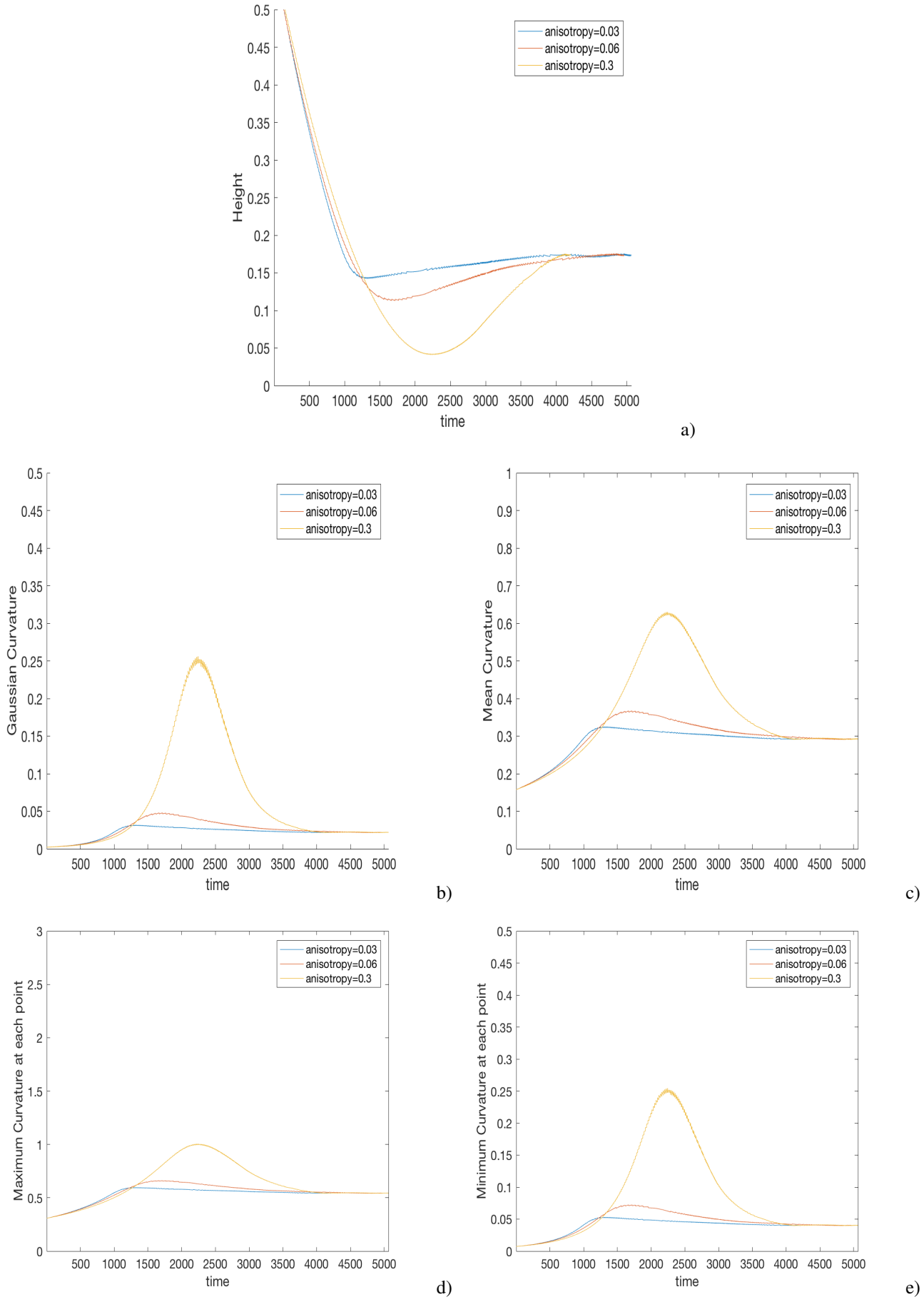

Fig. 7. Comparison of the behaviour of the change in height and different measures of curvature for different values of the anisotropy index: 0.3, 0.06 and 0.03. a) Height along the paths, b) Gaussian curvature along the paths, c) mean curvature along the paths. d) Maximum curvature at each point along the paths, and e) Minimum curvature at each point along the paths.

to appreciate that, from the left-bottom corner to the middle of the path, it tend to follows the level lines, thus, avoiding height changes. In the end, the path traverses a valley since the cost of going around this valley is higher. The third image (c) shows the tensorial field used as velocity (cost) function for the wavefront evolution, which is composed by ellipses whose main directions are those of the height larger (d) and smaller (e) gradient.

Finally, figure 9 shows an application of this method to a height map of an area of Mars which has many sandy dunes. When moving around this kind of environment, robots need to avoid the slopes of the terrain since it is very likely that they lose the control of the movement due to slips. In order for the paths to avoid these areas, an anisotropy coefficient of 0.03 is chosen. Figure 9 shows different paths computed using the AFM method from different initial positions to the same goal point. It is possible to appreciate that all of them only traverse areas in which there is a change of height when it is strictly necessary, such as when the path starts in the slope of a dune (darker areas).

Several tests on different environments have been carried out in order to test the usability of the algorithm and its results in different environments which provide insights to understand the behaviour of the algorithm according to the anisotropy index.

Figure 3 shows the adaptation of a path to the terrain following the tensorial field. It can be seen how the path has the least possible changes in height from the starting to the goal point. The first image shows the height map and the computed path. The second one includes the tensor field computed from the height map and based on its gradient, which is shown in the third image. In the fourth one the Normal components of the gradient are indicated. Finally, a 3D view of the environment and the computed path are included.

The adaptation to the terrain can be more or less strict depending on the anisotropy index set by the user. The next simulation shows how this index can influence the path computed by the algorithm. Figure 5 shows this influence using the next values for the Anisotropy index: 0.01, 0.03 and 0.05. The first image shows the path with less changes in height, however, the path includes abrupt turns. When the index is augmented, the path has more altitude changes but gets smoother, being the third best one the best option in this case, with index $a = 0.05$. Figure **??** shows the Different paths in the Mars dunes using the AFM method for an anisotropy coefficient of 0.03 and Figure 6 shows different paths in the uplift of layered materials from the intersection of two craters of Mars using the AFM method for an anisotropy coefficient of 0.03. Then, figure 10 includes: a) the height map of the environment with the computed Anisotropic Fast Marching path following the the peaks of the area; the mean curvature of the environment; and two quality measurements of the path shown in a), c) the height changes and d) the curvature changes along the path.

Figure 12 shows The adaptation of the AFM paths to the level lines is better when importance of the normal eigenvector field is higher (smaller anisotropy index). Left: Height of terrain that consists in mountain (upper view) and a typical path between two points and right: AFM expansion, normal vectorial field and path, for anisotropy indexes of 0.3, 0.06 and 0.03.

A. Pure Pursuit applied to AFM

To introduce the robot's kinematics in the method from the ideal trajectory for a robot point that gives us the AFM, we have implemented a Pure Pursuit algorithm. This algorithm keeps track of the route. To do this, it calculates the angular velocity that moves the robot from its current position to a point that is further along the path. The linear speed is assumed constant and therefore, it is only necessary to calculate the steering angle. Next, the algorithm moves the anticipation point of the path and so on until reaching the end point of the path. That is, the algorithm pursues a point that is moving in front of it. A fundamental parameter is the distance to the anticipation point, because if it is too small the robot tends to oscillate and if it is very large, the algorithm softens the trajectory too much.

In the figure ref afm20a you can see how the algorithm works. The input is the reference path obtained by AFM, the next block is the follower of the path, which uses the point of anticipation and whose output is the steering angle and the last block consists on the kinematic model of the robot.

Para modelar el robot se ha elegido un modelo simplificado del rover que es un vehiculo four-wheel-steering. Para ello se ha seguido el modelo cinematico de Wang [8].

Reference point C is chosen at the center of gravity of the vehicle body. Its coordinates (X,Y) represents the position of the vehicle; Vehicle Velocity v is defined at the reference point C; Heading Angle ψ is the angle from the X-axis to the longitudinal axis of the vehicle body AB; Course Angle γ is the angle from the X-axis to the direction of the vehicle velocity, v; Side-slip Angle β is the angle from the longitudinal axis of the vehicle body AB to the direction of vehicle velocity, v; Turning radius r is the distance between the reference point C and the Instant Rotating Center (IRC) O; Front Wheel Velocity vf is the velocity defined at the intersection of the mid-plane of the virtual front wheel and the front wheel axle, A; Rear Wheel Velocity vr is the velocity defined at the intersection of the mid-plane of the virtual rear wheel and the rear wheel axle, B; Front wheel steering angle δf is the angle from the longitudinal axis of the vehicle body AB to the direction of vf; Rear wheel steering angle δr is the angle from the longitudinal axis of the vehicle body AB to the direction of vr.

VII. Conclusion

The algorithm we have presented is a novel methodology for considering the most important aspects of path planning for exploration of planets or asteroids. The main characteristic considered is how to minimise the changes in height, i.e. to follow as much as possible the level curves and clearness among obstacles. In order to accomplished these goals, the Anisotropic Fast Marching Method has been used. Numerical simulations show promising results on the application of this methodology. Different results show the influence of the

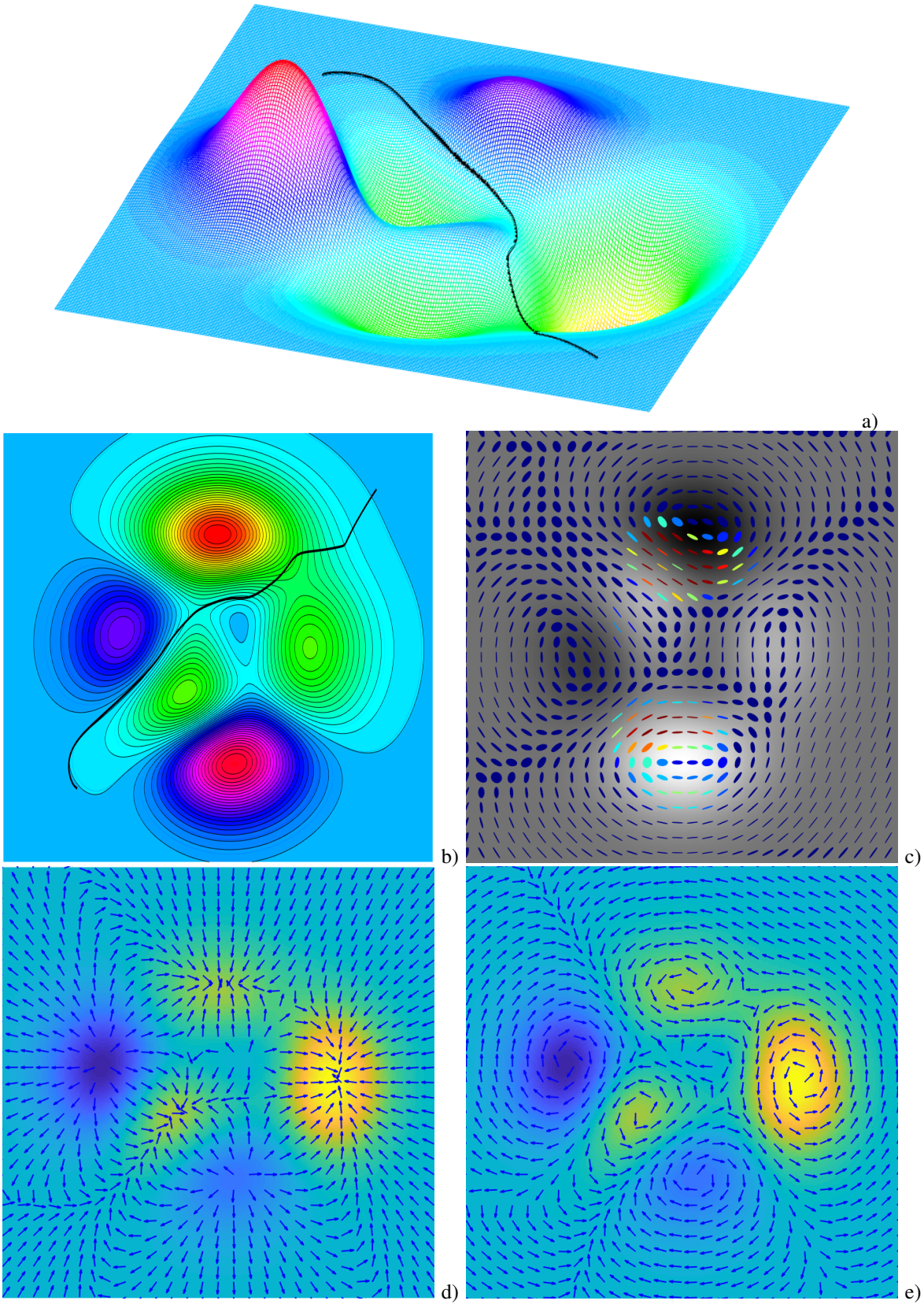

Fig. 8. a) Typical Anisotropic Fast Marching path with small changes in height, b) Tensorial field associated to this map, c) and d) Gradient and Normal components of the tensorial field, and e) 3D plot of the same path.

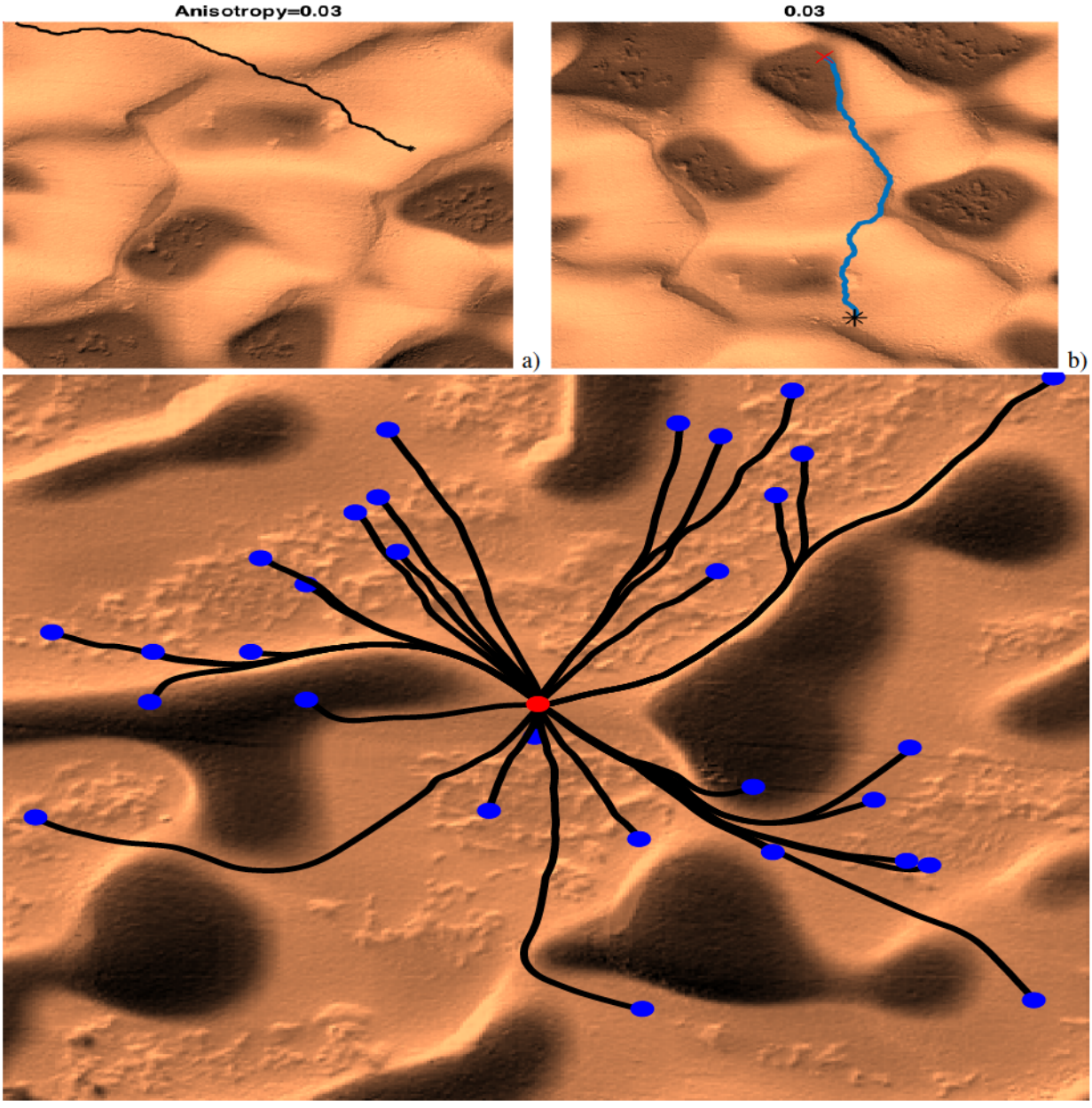

Fig. 9. Different paths calculated penalising the changes in height.

TABLE III
SUMMARY OF KINEMATICS MODEL EQUATIONS

Symbol	Nomenclature	Equation
X	Global X axis coordinate	$\dot{X} = V\cos(\psi+\beta)$
Y	Global Y axis coordinate	$\dot{Y} = V\sin(\psi+\beta)$
ψ	Yaw angle, orientation angle of vehicle with respect to global X axis	$\dot{\psi} = \frac{V\cos(\beta)}{l_f+l_r}(\tan(\delta_f) \quad \tan(\delta_r))$
β	Vehicle slip angle	$\beta = \tan^{1}\left(\frac{l_f\tan\delta_r+l_r\tan\delta_f}{l_f+l_r}\right)$

combination of several characteristics of the environment in the resulting path. In all cases, obstacles and difficult terrain are avoided.

REFERENCES

[1] Sethian, J.A.: Theory, algorithms and aplications of level set methods for propagating interfaces. Acta numerica, Cambridge University Press, pp. 309-395 (1996)
[2] Yatziv, L., Bartesaghi, A., Sapiro, G.: A fast o(n) implementation of the fast marching algorithm. J. of Computational Physics, vol. 212, pp. 393-399 (2005)
[3] J. Sethian, Level set methods, Cambridge University Press, 1996.
[4] Gómez, J.V., Álvarez, D., Garrido, S., Moreno, L.: Fast methods for eikonal equations: an experimental survey. ArXiV **abs/1506.03771** (2015).
[5] Vladimirsky, A., Sethian, J.A.: Ordered upwind methods for static Hamilton-Jacobi equation: Theory and algorithms. SIAM J. of Numerical Analysis, vol. 41, no. 1, pp. 325-0363 (2003)
[6] Peyre, G.: Advanced Signal, Image and Surface Processing. In: Ceremade, Université Paris-Dauphine (2010)

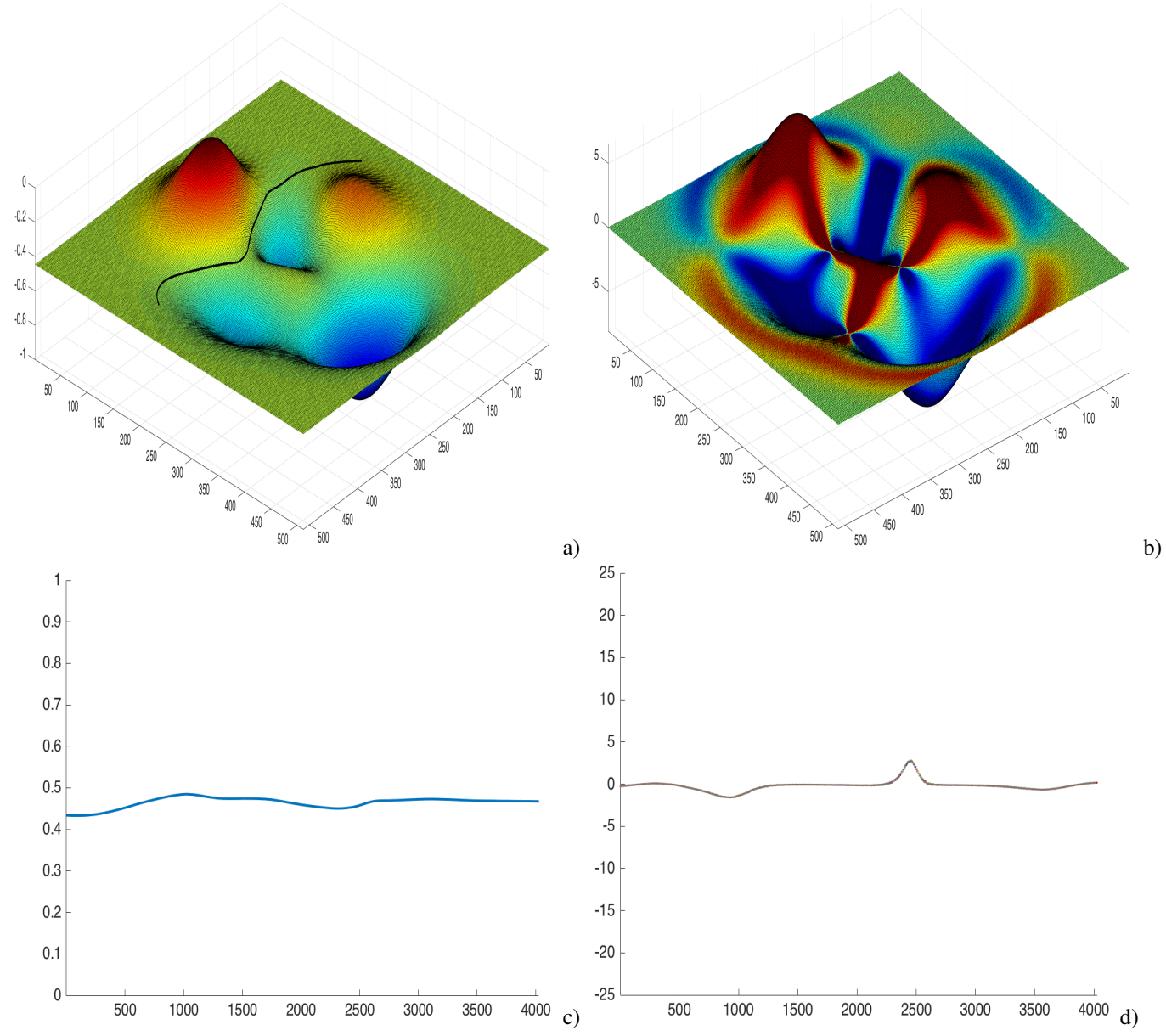

Fig. 10. a) Anisotropic Fast Marching path in the peaks artificial environment, b) Mean Curvature of the environment, c) Height changes along the path shown in a), and d) Curvature changes along the path shown in a).

[7] Valero-Gomez, A., Gomez, J.V., Garrido, S., Moreno, L.: The Path to Efficiency: Fast Marching Method for Safer, More Efficient Mobile Robot Trajectories. In: IEEE Robotics and Automation Magazine, vol. 20(4), pp.111-120 (2013)
[8] Wang, D. and Qi, F., "Trajectory planning for a four wheel steering vehicle," Proceedings of the 2001 IEEE International Conference on Robotics and Automation, Seoul, Korea, May 21-26, 2001.
[9] S. Garrido, L. Moreno, M. Abderrahim, D. Blanco, Fm2: A real-time nsensor-based feedback controller for mobile robots, International Journal of Robotics and Automation 24(1) (2009) 3169–3192.
[10] Kimmel, R., Sethian, J.A.: Computing geodesic paths on manifolds. In: The National Academy of Sciences, vol. 95 (1998)
[11] Weickert, J., Anisotropic diffusion in image processing. Teubner, 1998.
[12] Weickert, J., Visualization and Processing of Tensor Fields. Springer. 2005.

Santiago Garrido received the B.S. degree in mathematics from the Complutense University of Madrid, Madrid, Spain, the B.S. degree in physics science in the UNED and the Ph.D. degree in electrical, electronics and automation engineering from the Carlos III University of Madrid (UC3M), Madrid, in 2000. He joined the Department of Systems Engineering and Automation, UC3M, where he has been involved in several mobile robotics projects. His research interests include mobile robotics, mobile manipulators, environment modelling, sensor based robot motion, and mobile robot global localisation problems.

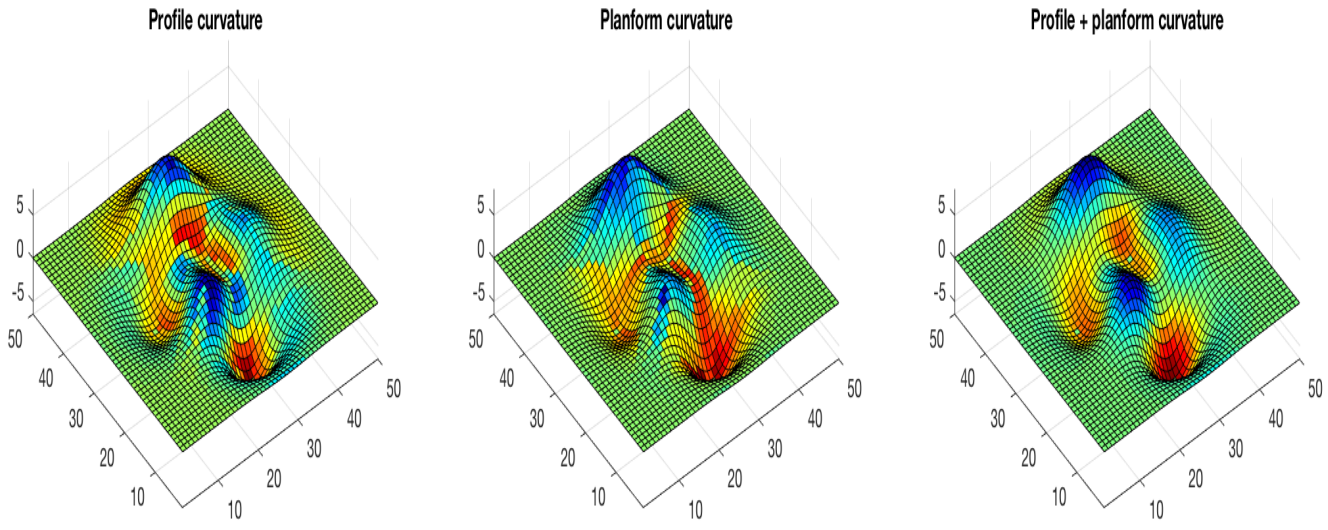

Fig. 11. Profile curvature is the curvature along the steepest downward gradient and planform curvature is the curvature perpendicular to the downward gradient.

Luis Moreno received the B.S. degree in automation and electronics engineering and the Ph.D. degree from the Universidad Politécnica de Madrid,Madrid, Spain, in 1984 and 1988, respectively. From 1988 to 1994, he was an Associate Professor with the Universidad Politécnica de Madrid. In 1994, he joined the Department of Systems Engineering and Automation, Carlos III University of Madrid (UC3M), Madrid, where he has been involved in several mobile robotics projects. His research interests include mobile robotics, mobile manipulators, environment modelling, path planning, and mobile robot global localisation problems.

Third C. Author, Jr. (M'87) received the B.S. degree in mechanical engineering from National Chung Cheng University, Chiayi, Taiwan, in 2004 and the M.S. degree in mechanical engineering from National Tsing Hua University, Hsinchu, Taiwan, in 2006. He is currently pursuing the Ph.D. degree in mechanical engineering at Texas A&M University, College Station, TX, USA.

From 2008 to 2009, he was a Research Assistant with the Institute of Physics, Academia Sinica, Tapei, Taiwan. His research interest includes the development of surface processing and biological/medical treatment techniques using nonthermal atmospheric pressure plasmas, fundamental study of plasma sources, and fabrication of micro- or nanostructured surfaces.

Mr. Author's awards and honors include the Frew Fellowship (Australian Academy of Science), the I. I. Rabi Prize (APS), the European Frequency and Time Forum Award, the Carl Zeiss Research Award, the William F. Meggers Award and the Adolph Lomb Medal (OSA).

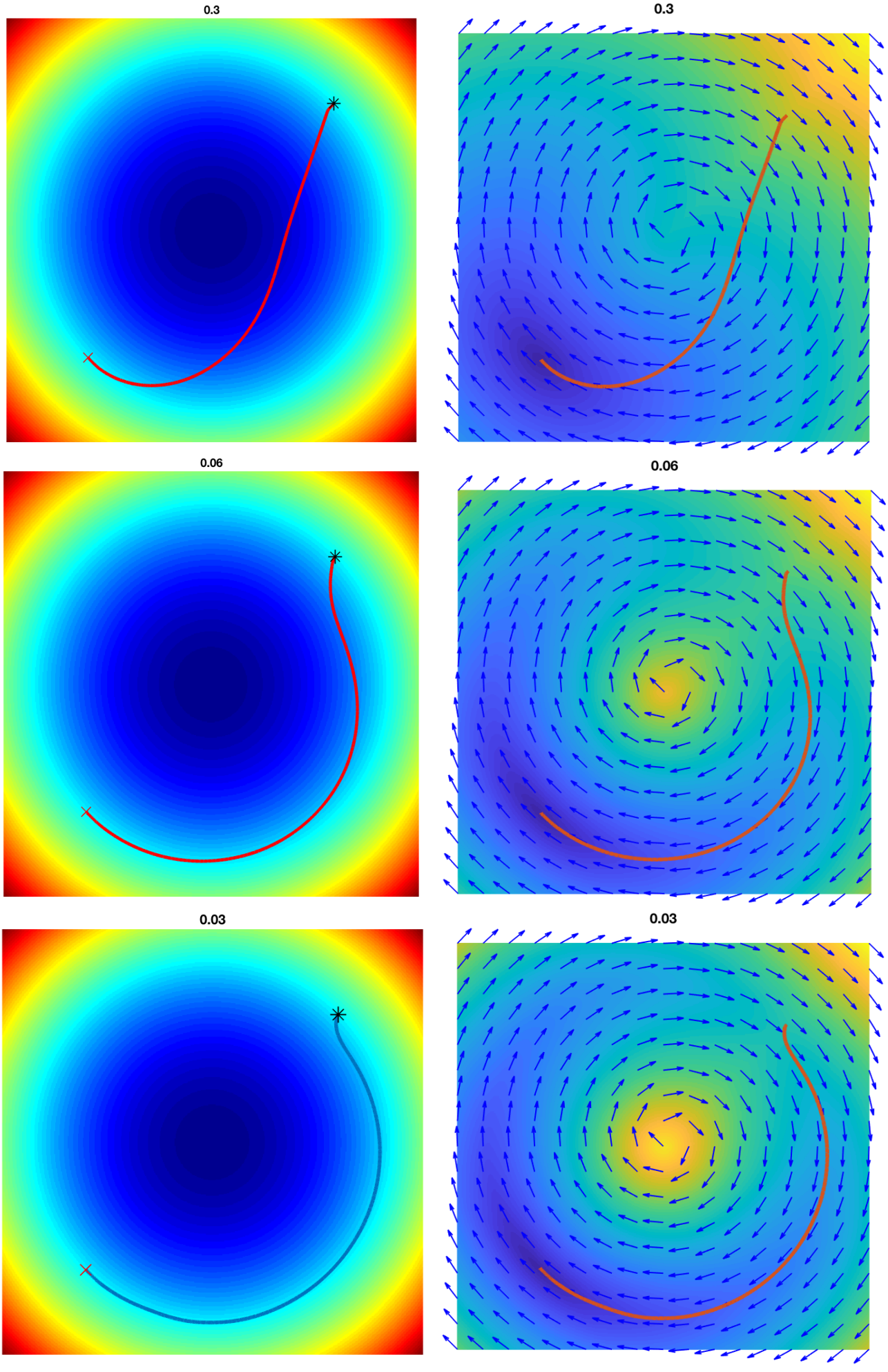

Fig. 12. The adaptation of the AFM paths to the level lines is better when importance of the normal eigenvector field is higher (smaller anisotropy index).

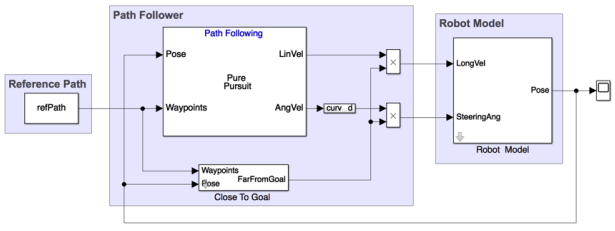

Fig. 13.

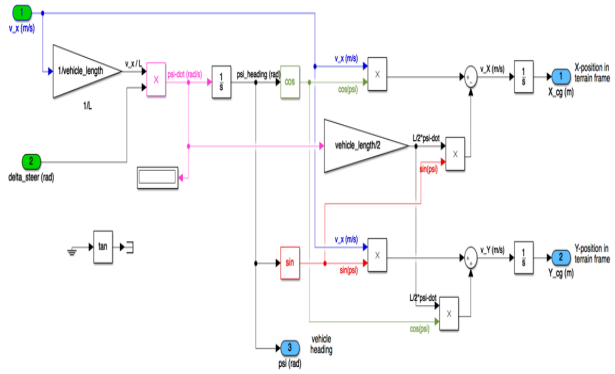

Kinematic vehicle model of wheelbase length L and width W.
Non-holonomic constraints on front and rear wheels allow rolling at low speed with no slipping:

$$v_X = [\, v_x \cdot \cos(\psi_{heading}) - (L/2) \cdot \omega_z \cdot \sin(\psi_{heading}) \,]$$
$$v_Y = [\, v_x \cdot \sin(\psi_{heading}) + (L/2) \cdot \omega_z \cdot \cos(\psi_{heading}) \,]$$

where:
v_x - body-fixed vehicle velocity
v_X - terrain frame X velocity
v_Y - terrain frame Y velocity
ψ-dot - same as ω_z
ψ-dot - $(v_x / L) \cdot \delta_{steer}$

Fig. 16.

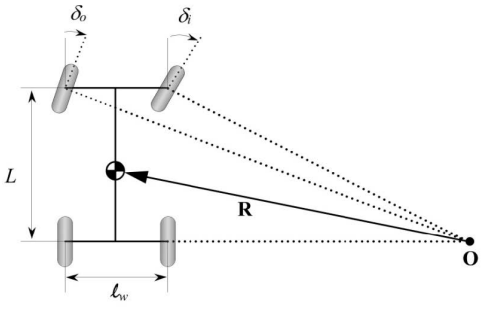

Fig. 14.

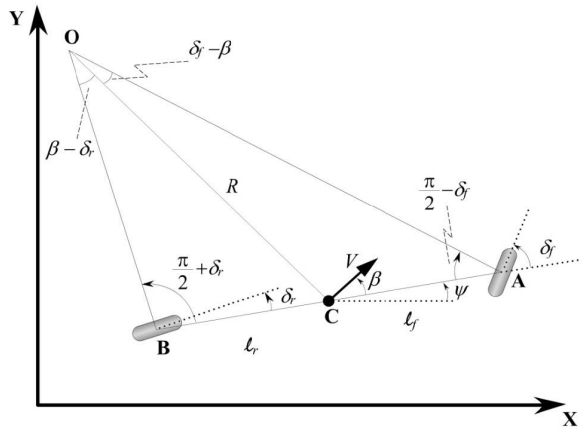

Fig. 15.

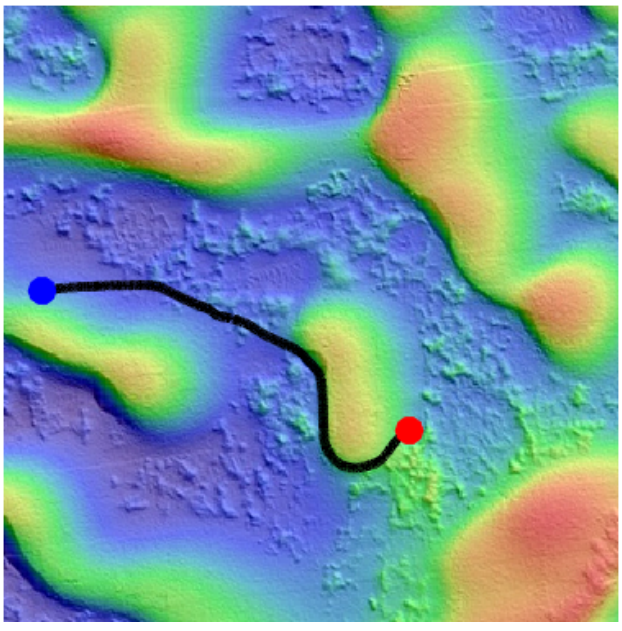

a)

Fig. 17.

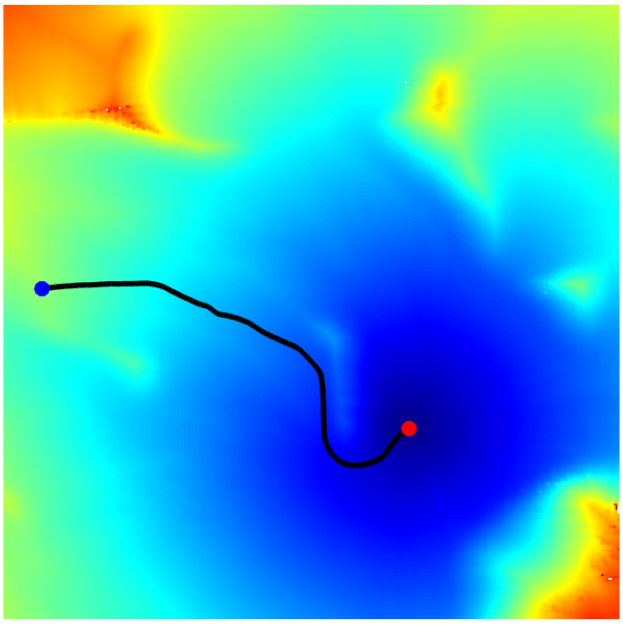

b)

Fig. 18.

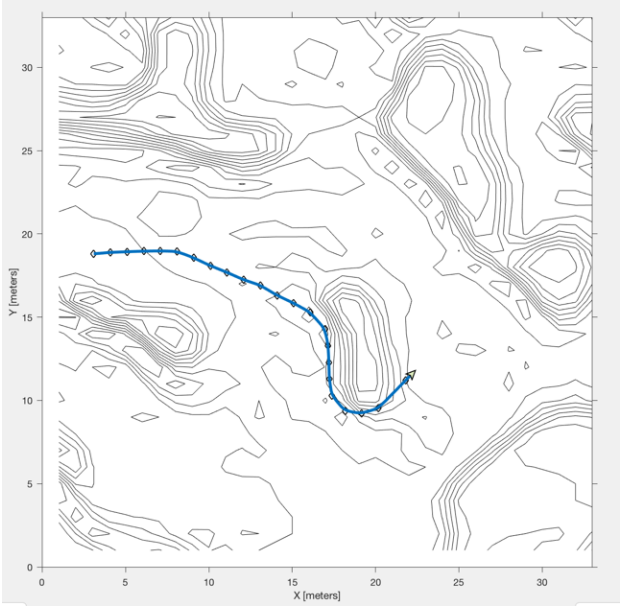

Fig. 19.